PAPER

Modeling the making and breaking of bonds as an elastic microcapsule moves over a compliant substrate

Egor A. Maresov,[a] German V. Kolmakov,[b] Victor V. Yashin,[a] Krystyn J. Van Vliet[c] and Anna C. Balazs[*a]

By integrating the lattice Boltzmann model for hydrodynamics, the lattice spring model for micromechanics of elastic solids, and the Bell model for bond formation and rupture, we examine the fluid driven motion of elastic microcapsules on compliant surfaces. The capsules, modeled as three-dimensional fluid-filled elastic shells, represent polymeric microcapsules or biological cells. We observed three regimes of capsule motion. Namely, the capsule rolls steadily along the substrate at a sufficiently high shear rate, it is stationary at a low shear rate, and exhibits an intermittent motion (saltation) at intermediate shear rates. At a given shear rate, the regime of capsule motion was found to depend on the substrate stiffness, and on the rate of rupture of the adhesive bonds. The capsule was observed to roll steadily on a sufficiently stiff substrate, and at a high rate of bond rupture. In the opposite limit of a soft substrate and low rate of bond rupture, the system was localized in the stationary regime. The findings provide guidelines for creating smart surfaces that could regulate the motion of the microcapsules.

1. Introduction

Polymeric microcapsules constitute ideal micro-carriers for a range of materials, from inks and flavorants, to cosmetics and drugs. These microcapsules permit the controlled release of the encapsulated species and thus, are useful in the food, chemical and pharmaceutical industries.[1] In the vast majority of these applications, the utility of the capsules comes from their binding to substrates, and consequently, releasing the encapsulated species at these surfaces. For example, for the targeted delivery of drugs, dyes or flavorings, the capsules must bind to an interface in order to be effective. In this binding process, the mechanical compliance of both the capsule and the substrate can have a significant effect. For instance, the contact area between a compliant capsule and a surface will be greater than the contact area between a stiff capsule and that surface; hence, the more compliant capsule could be more effective in the delivery process. Similarly, a more compliant substrate can be more effective at binding the capsules and thus, improving the utility of the delivery device.

Another important component in the technological uses of polymeric microcapsules[1] (as well as other micro-carriers, such as liposomes[2] and polymersomes[3]) is an imposed flow field; for example, blood flow plays a vital role in the effectiveness of

microcapsules used for drug delivery. Thus, to enhance the efficacy of these micro-carriers, it becomes important to determine how the combined effects of the flow field, the compliance of the capsule, the elasticity of the substrate and binding interactions between the capsule and substrate contribute to the performance of the system. Given this number of critical variables, computational modeling provides an effective approach for pinpointing the factors that influence the system's behavior.

Herein, we take advantage of our recently developed hybrid "LBM/LSM" computational approach[4–9] to model a microcapsule as a fluid-filled, elastic shell and simulate the effects of an external fluid on the motion of this capsule on a flexible substrate. In our hybrid approach, we integrate two mesoscopic lattice models, the lattice Boltzmann model (LBM) and the lattice spring model (LSM), which can be used to simulate the underlying processes that give rise to the appropriate continuum behavior. In particular, the fluid dynamics is captured *via* the LBM, which can be viewed as an efficient solver for the Navier–Stokes equation. More specifically, the LBM incorporates the mesoscopic physics of fluid "particles" propagating and colliding on a cubic lattice such that the averaged, long-wavelength properties of the system obey the desired Navier–Stokes equation.[10]

The behavior of the capsule's elastic shell is simulated using the LSM. In the LSM, an elastic material is modeled through a network of interconnected harmonic "springs", which describe the interactions between neighboring sites. The mechanical properties of this material (*e.g.*, the Young's modulus) can be expressed in terms of the spring constants of the harmonic springs and the spacing between the lattice sites. Notably, the

[a]*Chemical Engineering Department, University of Pittsburgh, Pittsburgh, PA, 15261, USA*
[b]*Department of Physics, New York City College of Technology, City University of New York, Brooklyn, NY, 11201, USA*
[c]*Materials Science and Engineering Department, Massachusetts Institute of Technology, Cambridge, MA, 02139, USA*

large scale behavior of the resultant system can be mapped onto continuum elasticity theory.[11]

Our integrated LBM/LSM approach allows for a dynamic interaction between the elastic walls and the surrounding fluid. In other words, dynamically and interactively, the moving walls exert a force on the fluid and, in turn, the fluid reacts back on the walls. In this manner, we can model the complex fluid-structure interactions that occur at the boundaries between the fluid and the compliant surfaces (*i.e.*, the capsule's elastic shell and the soft substrate). We have validated our three-dimensional (3D) LBM/LSM model by determining the drag force on a periodic array of spheres, as well as simulating the breathing mode oscillations of a single capsule.[4] In both cases, the simulations showed quantitative agreement with analytical theory.[4]

In our previous LBM/LSM simulations of the motion of fluid-driven capsules on adhesive surfaces,[4–9] we used the Morse potential to model the binding interactions between the capsule and substrate. Herein, we modify our approach by integrating the Bell model[12] into the LBM/LSM to describe the formation and rupture of chemical bonds between the compliant capsule and soft substrate. The Bell model allows us to take into account the effect of an applied force (arising, for example, from an imposed flow) on the rupture of the bonds. Furthermore, we can ascribe a degree of chemical specificity to the bonds formed between the capsules and substrate. As detailed in the *Methodology* section, the rupture rate, k_r, is an exponential function of the force applied to the bond between the capsule and the substrate. The rupture rate is also directly proportional to the off-rate constant, k_{off}, which is an intrinsic characteristic of a chemical bond. By specifying the value of k_{off}, we can ascribe a specific chemical character to the bond between the capsule and surface.

Notably, the Bell model has been used successfully to describe ligand-receptor interactions between biological interfaces. In particular, Hammer *et al.*[13] have pioneered the use of the Bell model to simulate the dynamic interactions of leukocytes rolling on rigid surfaces and showed how the behavior of the leukocytes depended on the applied force and relevant rate constants. In the latter studies, the leukocytes were modeled as rigid spheres. More recently, researchers have modeled the leukocytes as compliant capsules.[14,15] Nonetheless, in these different studies, the substrates were modeled as rigid surfaces.

To the best of our knowledge, the studies described herein constitute the first simulations of the interactions between mobile, compliant capsules and soft surfaces that interact through Bell bonds. These studies not only provide insight into the dynamic behavior of microcapsules on flexible substrates, but also can shed light on the factors that contribute to regulating the interactions between biological cells, such as leukocytes, and compliant interfaces. Below, we demonstrate that the compliance of the substrate can have a significant effect on the motion of the capsules. Furthermore, by examining the behavior of the system at different values of the shear rate, the Young's moduli of both the substrate and the capsule, and the chemical binding constants, we show that judicious choices in the parameter space allow one to either localize the capsule at a fixed site on the surface or drive the micro-carrier to roll along the interface. Given that different applications might necessitate different behavior, the findings provide guidelines for tailoring the system to exhibit the desired performance.

Below, we first describe our computational approach and then discuss our findings on the sensitivity of the dynamic behavior of the microcapsules to the properties of its local environment.

2. Methodology

2.1 Model

We use our hybrid LBM/LSM approach to simulate a fluid-filled, three-dimensional capsule, which is immersed in a host fluid and localized on a compliant substrate (Fig. 1). Due to an imposed shear flow, the capsule can be driven move along the substrate. The capsule's elastic, solid shell is modeled *via* the lattice spring model (LSM), which consists of a triangular network of harmonic springs connecting regularly spaced mass points, or nodes.[4–9,11,16] The spring force $\mathbf{F}_s$ on node $\mathbf{r}_i$ is equal to

$$\mathbf{F}_s(\mathbf{r}_i) = -\sum_j k_j [(r_{ij} - r_{ij}^{eq})/r_{ij}] \, \mathbf{r}_{ij} \qquad (1)$$

where the summation runs over the nodes that are connected to the ith node by the springs. The quantity $\mathbf{r}_{ij} = \mathbf{r}_i - \mathbf{r}_j$ is the radius vector between ith and jth nodes, r_{ij}^{eq} is the equilibrium length of the spring and k_{ij} is the spring constant. To capture the dynamics of the solid shell, we numerically integrate Newton's equations of motion, $M \, d^2\mathbf{r}_i/dt^2 = \mathbf{F}(\mathbf{r}_i)$, where M is the mass of a node. Upon transforming the equations to the dimensionless form, the mass of a node is taken to be $M = 1$. The total force $\mathbf{F}$ acting on a node consists of the following: the sum of the spring forces between the masses (representing the elastic response of the solid shell), the force exerted by the fluid on the shell at the fluid-solid boundary, and the adhesion forces at the compliant substrate (see below).

The capsule's spherical shell is formed from three concentric layers of the LSM nodes. The layers were generated by triangulation of a sphere and each layer contains $N = 642$ nodes. The nodes within a layer are connected by springs along the edges of the triangles, and each node in a layer is connected by springs to several neighboring nodes in an adjacent layer. Hence, the shell contains a total of 14,724 springs. The distance between the layers of the shell is $1.5 \, \Delta x_{LBM}$, where Δx_{LBM} is the spacing in the
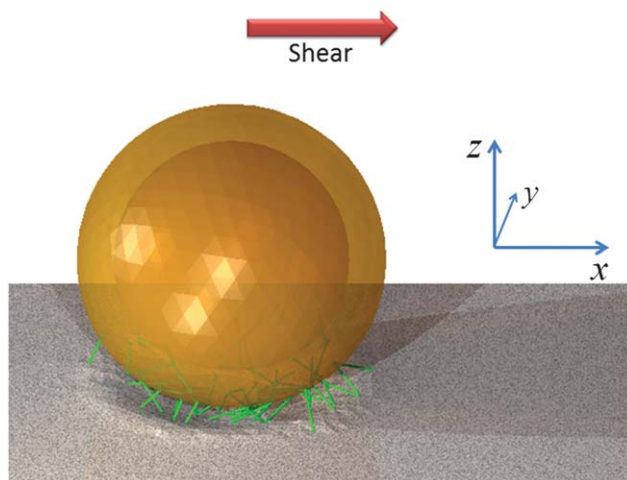

Fig. 1 An elastic capsule adhered to a compliant substrate and surrounded by fluid with an imposed shear flow. The green lines represent the adhesive bonds formed between the capsule and substrate.

lattice Boltzmann model LBM (see below), so that the capsule thickness is $h = 3 \Delta x_{LBM}$. (The distance between the layers of the shell was chosen to be similar to the mean length of the springs within a layer to maintain the isotropic nature of the elastic properties.) The outer radius of the shell was taken to be $R = 12.5 \Delta x_{LBM}$.

All springs in the capsule have the same spring constant k_{cap}, and the equilibrium length of a spring is equal to the distance between the two corresponding nodes in the undeformed state. Note that the springs can differ in their equilibrium length because they are used to model an intrinsically curved object (capsule). For small deformations, the LSM obeys linear elasticity theory and all the macroscopic elastic properties, such as the Young's modulus, shear modulus, bending rigidity, *etc.*, are expressed in terms of the spring constants, nodal masses, and the lattice geometry.[11,16,17] In particular, the Young's modulus of the capsule's shell can be estimated as $E_{cap} \approx 5k_{cap}/2l_{cap}$,[11] where $l_{cap} \approx 1.94 \Delta x_{LBM}$ is the average equilibrium length of the springs. (We note that in order to avoid numerical fluctuations in the forces acting on the solid nodes,[4,8,16] the respective LSM and LBM spacing should be chosen such that $l_{cap} \geqslant \Delta x_{LBM}$.)

The elastic substrate is modeled *via* a cubic lattice of LSM nodes, with the spacing between these nodes being Δx_{LSM}. The springs connect the nearest and next-nearest nodes and thus, have equilibrium lengths of Δx_{LSM} and $\sqrt{2} \Delta x_{LSM}$, respectively; the respective spring constants are k_{sub} and $k_{sub}/2$. The resulting Young's modulus of the substrate is $E_{sub} = 5k_{sub}/2 \Delta x_{LSM}$.[11] We took $\Delta x_{LSM} = \Delta x_{LBM}$ in the simulations.

The dynamics of the host fluid and the fluid within the capsule are simulated using the lattice Boltzmann model (LBM). The LBM can be viewed as an efficient solver for the Navier–Stokes equation.[10] Specifically, this lattice-based model consists of two processes: the propagation of fluid "particles" to neighboring lattice sites, and the subsequent collisions between particles when they reach a site. These fluid particles are representative of mesoscopic portions of the fluid, and are described by a particle distribution function $f_i(\mathbf{r},t)$, which characterizes the mass density of fluid particles at a lattice node $\mathbf{r}$ and time t propagating in the direction i with a constant velocity $\mathbf{c}_i$. The velocities $\mathbf{c}_i$ in the ith direction are chosen so that fluid particles propagate from one lattice site to the next in exactly one LBM time step, Δt_{LBM}.

The time evolution of these distribution functions is governed by a discretized Boltzmann equation.[10] To model the three-dimensional system, we use the 3DQ19 scheme, which involves a set of 19 particle velocity distribution functions at each node, and the single relaxation time approximation (the LBGK scheme).[18] The hydrodynamic quantities of interest are the moments of the distribution function, *i.e.*, the mass density $\rho = \sum_i f_i$, the momentum density $\mathbf{j} = \rho \mathbf{u} = \sum_i \mathbf{c}_i f_i$, with $\mathbf{u}$ being the local fluid velocity, and the momentum flux $\Pi = \sum_i \mathbf{c}_i \mathbf{c}_i f_i$.

In our LBM/LSM simulations, the fluid and solid phases interact through appropriate boundary conditions.[4,5,16] In particular, the lattice spring nodes that are situated at the solid-fluid interface impose their velocities on the surrounding fluid; the velocities are transmitted through a linked bounce-back rule[19] to those LBM distribution functions that intersect the moving solid boundary. In turn, the LSM nodes at the solid-fluid interface experience forces due to the fluid pressure and viscous stresses at that boundary. We calculate the latter force based on the momentum exchange between the LBM particle and the solid boundary, and then distribute this quantity as a load to the neighboring LS nodes. This scheme provides a means of implementing no-slip boundary conditions at the fluid-solid interface.

The capsule binds to the substrate through the formation of bonds that mimic the ligand-receptor interactions in biological systems. Each node on the capsule's outer surface can form a bond with each substrate node if the distance between the two nodes, r, is shorter than a certain cut-off radius, r_{cut}. When the bond is formed, the interaction between the two nodes is described by the Hookean spring potential

$$U_{bond}(r) = 1/2 \, \kappa(r - l_{eq})^2, \qquad (2)$$

where κ is the bond spring constant, and l_{eq} is the length of an undeformed bond. The cut-off radius is taken to be $r_{cut} = 2l_{eq}$. To prevent any overlap between the capsule and substrate, we assume that the capsule and substrate nodes interact through the following short-range repulsion:

$$U_s(r) = u_s \exp(-r/l_s) \qquad (3)$$

Here, u_s and l_s are the respective strength and length of the repulsion; in the simulations, we set $l_s = 0.75 \, \Delta x_{LBM}$ and $u_s = 14.4 \kappa \Delta x_{LBM}^2$. We note that the potential $U_s(r)$ mimics the repulsive part of the Morse potential.[20]

The bonds between the capsule and substrate can break and reform repeatedly. We utilize the Bell model[12,13] to simulate the stochastic processes of bond rupture and reforming. The Bell model serves as a useful framework for describing the relationship between bond dissociation and force.[21–23] The Bell model has been used widely to describe bonding interactions in various biological systems; for example, the model was utilized in characterizing the mechanical behavior of biological tissue,[24] the unfolding of proteins,[25] viral attachment,[26,27] and adhesion of cells to surfaces.[28–30] In the Bell model, the rupture rate constant, k_r, is an exponential function of the force F applied to the bond, $k_r = k_{off} \exp(r_0 F/k_B T)$. Here, k_{off} is the rupture rate constant of an unstressed bond (the off-rate), the parameter r_0 characterizes the sensitivity of the bond to stress, k_B is the Boltzmann constant, and T is temperature. The force acting on a bond depends on the bond length, *i.e.*, on the distance between the nodes, r, and is calculated by differentiating eqn (2) to obtain the following expression for the distance-dependent rate constant of rupture:

$$k_r(r) = k_{off} \exp[r_0\kappa(r - l_{eq})/k_B T], \qquad (4)$$

The distance-dependent rate constant of bond reforming, $k_f(r)$, for a broken bond is determined from the principle of detailed balance as[13]

$$\frac{k_f(r)}{k_r(r)} = \frac{k_{on}}{k_{off}} \exp[-U_{bond}(r)/k_B T] \qquad (5)$$

In the above equation, $U_{bond}(r)$ is given by eqn (2), and k_{on} is the rate constant of bond formation (the on-rate).

2.2 Model parameters

Typical radii of polyelectrolyte multilayer microcapsules are in the range of 0.5 to 10 μm.[1,31] In our simulations, we assume the radius

of capsule to be of $R = 10$ μm, so the LBM spacing corresponds to $\Delta x_{LBM} = 0.8$ μm since we take $R = 12.5 \, \Delta x_{LBM}$ (see above). The LBM viscosity is given as $\mu = 1/6 \, \Delta x_{LBM}^2 \Delta t_{LBM}^{-1}$.[10] We assume that in the dimensional units, the viscosity is equal to that of water at the room temperature, $\mu = 10^{-6}$ m^2 s^{-1}, so one time step of the LBM corresponds to $\Delta t_{LBM} = 1.07 \times 10^{-7}$ s.

The fluid is located in a channel of thickness $H = 45 \, \Delta x_{LBM}$, which corresponds to the distance between the substrate and the top of the simulation box. The shear flow is generated by assigning a constant value to the fluid velocity in the X direction at the top LBM nodes; we refer to this as the wall velocity, V_w. The shear rate $\dot{\gamma}$ was varied from 2×10^{-7} to 4×10^{-6} Δt_{LBM}^{-1}. A wall velocity of $V_w = 1 \times 10^{-4}$ $\Delta x_{LBM} \Delta t_{LBM}^{-1}$ corresponds to a shear rate of $\dot{\gamma} = V_w/H = 2.2 \times 10^{-6}$ Δt_{LBM}^{-1}, or 20.1 s^{-1} in the dimensional units, and a Reynolds number Re $= R V_w/\mu = 7.5 \times 10^{-3}$. In what follows, the shear rate 20.1 s^{-1} is taken as the reference value, and is denoted $\dot{\gamma}_0$. It is worth noting that the value of $\dot{\gamma}_0 = 20.1$ s^{-1} lies within the range of shear rates used in experimental studies of capsules and biological cells; the latter range typically varies from 5 to 400 s^{-1}.[1]

It is convenient to characterize the rigidity of capsule by the dimensionless capillary number Ca $= \rho \mu V_{cap}/E_{cap}h$, where ρ and V_{cap} are the respective fluid density and capsule velocity. The capillary number Ca represents the relative importance of the viscous stress and the elastic stress on the capsule's shell. The capillary number for rigid, essentially non-deformable capsules[6] is typically on the order of Ca $< 10^{-3}$. Here, we use Ca $\sim 10^{-2}$, which corresponds to a capsule that is slightly deformable under a viscous stress. At the shear rate of $\dot{\gamma}_0 = 2.2 \times 10^{-6}$ Δt_{LBM}^{-1}, the capillary number in our system is Ca $= 2.05 \times 10^{-2}$.

The rigidity of the substrate was taken to be considerably lower than that of the capsule. The relative substrate modulus $E = E_{sub}/E_{cap}$ was varied from 0.024 to 0.121.

The strength of the capsule-substrate adhesive interactions relative to the elastic stress in the capsule is controlled by the dimensionless parameter $\Phi = \kappa N/E_{cap}h$, where k is the bond spring constant and N is the total number of nodes on the shell surface. We set $\Phi = 0.62$ in the simulations, so the adhesion strength was comparable to the elastic stresses in the capsule's shell.[4]

The rate constant of bond rupture k_{off} was varied from 3.3×10^{-6} to $1/6 \times 10^{-4}$ Δt_{LBM}^{-1}. In the dimensional units of time, the latter value equals 156 s^{-1} and corresponds to a bond energy of 25 $k_B T$, which is characteristic of some ligand-receptor interactions, such as avidin–iminobiotin,[32] and for the thiol/disulfide exchange reaction.[33] The value $k_{off} \sim 10^2$ s^{-1} is also characteristic of other biological binding interactions.[34–36]

In contrast to k_{off}, the value of the on-rate k_{on} is not as readily evident from experimental studies. It is usually taken to be one to four orders of magnitude greater than k_{off}. For example, the value of $k_{on} = 35k_{off}$ was used for interpreting the experimental data on the E-selectin/sLe^x pair.[14] In our simulations, the rate constant of the bond formation was taken to be $k_{on} = 1 \times 10^{-3}$ Δt_{LBM}^{-1}, so that the ratio k_{on}/k_{off} was in the range of 60 to 250.

2.3 Computer simulations

The LBM simulation box consisted of $70 \times 40 \times 46$ nodes in the XYZ directions, respectively. The shear flow was generated by setting the X component of fluid velocity to a constant value of V_W at the top LBM nodes. The boundary conditions for the LBM simulations were periodic in the X and Y directions. The mid-grid bounce back scheme was used to approximate the no-slip boundary conditions at the fluid-solid interface, as discussed above. The reversed propagation scheme was employed for the purpose of parallelization.[37] We note that the forces and fluid velocities are averaged over two successive LBM steps to eliminate potential numerical instabilities in the simulations.[38] (Other stabilization techniques can also be used to address this issue.[39])

The cubic lattice for modeling the elastic substrate *via* the LSM consisted of $72 \times 42 \times 9$ nodes in the XYZ directions, respectively. The LSM lattice was shifted relative to the LBM nodes by $\Delta x_{LSM}/2$ in all three directions. The bottom nodes of the substrate lattice were fixed in space. The top nodes of the substrate were subject to the forces due to the hydrodynamic and substrate-capsule interactions. Free boundary conditions were applied to the LSM nodes of substrate at the vertical edges of the sample, so that these edges were allowed to move without specific constrictions. It is worth noting that the LSM lattice is sufficiently wide that the capsule remains far from the substrate's edges during the simulation.

Newton's equations of motion for the LSM nodes in the substrate and capsule were integrated numerically using the fourth order Runge–Kutta algorithm with the time step Δt_{LBM}.

The capsule and substrate interact though the chemical bonds, eqn (2), and the repulsive potential, eqn (3). Reshuffling of the Bell bonds was performed every time step of the LBM simulations. The probability of a connected bond to break and the probability of a broken bond to reform during the time step Δt_{LBM} were taken to be of the following forms:

$$\begin{aligned} w_r &= 1 - \exp(-k_r \Delta t_{LBM}), \\ w_f &= 1 - \exp(-k_f \Delta t_{LBM}), \end{aligned} \quad (6)$$

where the values of k_r and k_f were computed according to eqn (4) and (5).

Each simulation run was initiated by establishing the equilibrium adhesion contact between the capsule and substrate for the given set of model parameters. For this purpose, the undeformed, spherical capsule was put into the quiescent fluid (*i.e.*, the LBM and upper wall velocities were zero) close to the substrate so that the bonds could form. Due to this bond formation, the capsule moves toward the substrate. During the equilibration, the capsule assumes its equilibrium shape and the velocities of the capsule's center of mass and surrounding fluid gradually decrease. The shear flow was initiated by setting the velocity V_W of the upper LBM nodes at the time $t_{start} = 1.5 \times 10^5$ Δt_{LBM}, which is equivalent to 0.016 s (see Fig. 2). The total duration of a simulation run was 2×10^6 Δt_{LBM}, or 0.21 s in the dimensional units.

Finally, the physical and the computational parameters of our model are summarized in Table 1.

3. Results and discussion

3.1 Three regimes of capsule motion

The above computational model was used to investigate the dynamic behavior of the fluid-driven capsules for a range of
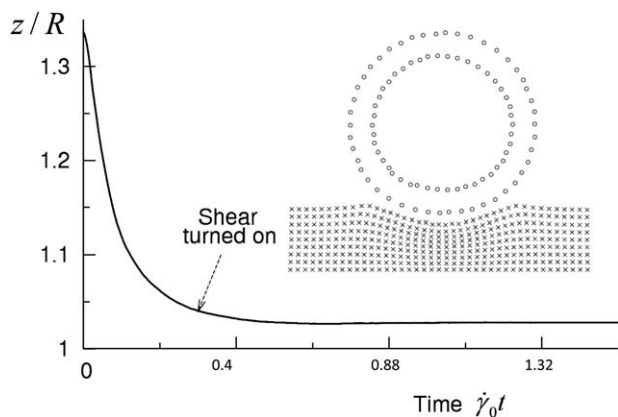
Fig. 2 The vertical position of the capsule's shell center of mass as a function of time. The shear flow is imposed at $t_{start} = 1.5 \times 10^5 \, \Delta t_{LBM}$. The inset shows the LSM nodes of the substrate and capsule (internal and external layers only) at t_{start}.

shear rates. *Via* these simulations, we observed three distinct types of dynamic behavior, which are characterized in Fig. 3. In particular, the plots in Fig. 3a and 3b show the respective displacement and velocity of the capsule's center of mass as a function of time t for three values of shear rate (indicated in the figure); the interaction strength and rate of bond rupture are fixed at $\Phi = 0.62$ and $k_{off} = 1.67 \times 10^{-5} \, \Delta t_{LBM}^{-1} = 7.6 \dot{\gamma}_0$, respectively. As seen in Fig. 3, for the lowest shear rate considered here, $\dot{\gamma} = 0.10 \dot{\gamma}_0$, the capsule is in the "stationary" state, *i.e.*, the capsule's position does not change with time (Fig. 3a) and its

velocity fluctuates near zero (Fig. 3b). For an intermediate value of shear rate, $\dot{\gamma} = 0.19 \dot{\gamma}_0$, a capsule can exhibit a cycle of "stop and start" behavior, where the capsule is stationary for a period of time, but then is driven to move for a finite time by the imposed flow. This "stop-and-start" phenomenon, referred to as "saltation", has been detected in experimental studies of leucocytes.[40,41] Saltation was also observed in the computer simulations of capsules driven to move along a rigid surface by an imposed shear flow.[15] It is important to recall that in contrast to the previous studies, we are modeling the rolling of capsules along a *compliant* substrate. Finally, at the sufficiently higher shear rate of $\dot{\gamma} = 0.6 \dot{\gamma}_0$, the capsule moves continuously (*i.e.*, travels from left to right in our simulation, with a steady increase in its x-coordinate), as shown in Fig. 3a. The velocity of the moving capsule fluctuates around some positive value (see Fig. 3b).

The continuously moving capsule undergoes a rolling motion on the substrate. Fig. 4 shows the velocity profiles v_{fluid} and v_{caps} for the fluid and capsule, respectively, at $t = 1.1 \times 10^6 \, \Delta t_{LBM}$ or $\dot{\gamma}_0 t = 2.4$, which corresponds to the middle of the simulation run. The fluid velocity profile $v_{fluid}(z)$ was obtained by averaging the x-component of the fluid velocity, $v_x(x,y,z)$, along nodes in the y-direction at $x = 0$ and a given value of z. To obtain $v_{caps}(z)$, the x-component of the velocity of the capsule shell nodes was averaged over the nodes having the z-coordinate within the interval from z to $z + \Delta x_{LBM}$. As seen in Fig. 4, the capsule velocity v_{caps} is close to zero near the substrate surface at $z = 0$, and increases with an increase in z. The latter behavior of v_{caps} as a function of z indicates that the capsule is undergoing a rolling

Table 1 Nomenclature and parameters used in the simulation

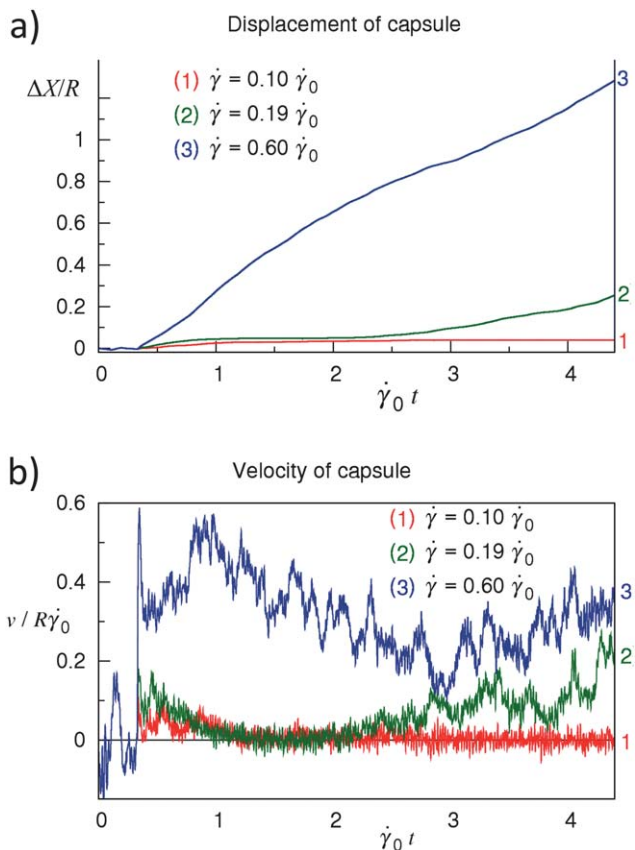|	
LBM	
Lattice spacing	$\Delta x_{LBM} = 0.8 \, \mu m$
Time step	$\Delta t_{LBM} = 1.07 \times 10^{-7} \, s$
Simulation box	$70 \times 40 \times 46 \, (\Delta x_{LBM})^3$
Unperturbed height of channel	$H = 45 \, \Delta x_{LBM}$
Capillary number	$Ca = \rho \mu V_{cap}/E_{cap} h \sim 10^{-2}$
Shear rate	$\dot{\gamma} = 2 \times 10^{-7} - 4 \times 10^{-6} \, \Delta t_{LBM}^{-1}$
Reference value	$\dot{\gamma}_0 = 2.2 \times 10^{-6} \, \Delta t_{LBM}^{-1} \sim 20.1 \, s^{-1}$
Reynolds number	$Re = RV_w/\mu \sim 10^{-3} - 10^{-2}$
Kinematic viscosity	$\mu = (1/6) \, \Delta x_{LBM}^2 \, \Delta t_{LBM}^{-1} \, \mu = 10^{-6} \, m^2 \, s^{-1}$
LSM	
Mass of a node	m_{LSM}
Capsule	
Radius	$R = 12.5 \, \Delta x_{LBM} = 10 \, \mu m$
Shell thickness	$h = 3 \, \Delta x_{LBM}$
Number of nodes (per each of 3 layers)	$N = 642$
Average equilibrium spring length	$l_{cap} \approx 1.94 \, \Delta x_{LBM}$
Spring constant	$k_{cap} = 0.8 \times 10^{-4} - 1.0 \times 10^{-4} \, m_{LSM} \, \Delta t_{LBM}^{-2}$
Substrate	
Lattice size	$72 \times 42 \times 9 \, (\Delta x_{LBM})^3$
Equilibrium spring length	$\Delta x_{LSM} = \Delta x_{LBM}$
Spring constant	$k_{sub} = 2 \times 10^{-6} - 5 \times 10^{-6} \, m_{LSM} \, \Delta t_{LBM}^{-2}$
Relative stiffness (Young's modulus)	$E = E_{sub}/E_{cap} = 0.024 - 0.121$
Adhesion	
Bell bonds (eqn (4), 5)	
Off-rate of unstressed bonds	$k_{off} = 3.3 \times 10^{-6} - 1/6 \times 10^{-4} \, \Delta t_{LBM}^{-1} = 1.5 - 7.6 \dot{\gamma}_0$
On-rate of unstressed bonds	$k_{on} = 1 \times 10^{-3} \, \Delta t_{LBM}^{-1} = 4.5 \times 10^2 \dot{\gamma}_0$
Equilibrium length	$l_{eq} = 2 \, \Delta x_{LBM}$
Spring constant	$\kappa = 3 \times 10^{-7} \, m_{LSM} \, \Delta t_{LBM}^{-2}$
Sensitivity to strain	$r_0 \kappa / k_B T = 0.9 \, \Delta x_{LBM}^{-1}$
Nonspecific repulsion (eqn (3))	
Length	$l_s = 0.75 \, \Delta x_{LBM}$
Respective strength	$u_s = 14.4 \, \kappa \, \Delta x_{LBM}^2$

Fig. 3 The three regimes of the capsule's motion observed in the simulations. (a) Displacement of the capsule's shell center of mass as a function of time corresponding to (1) the stationary state at $\dot{\gamma} = 0.1\dot{\gamma}_0$, (2) the intermittent regime (saltation) at $\dot{\gamma} = 0.19\dot{\gamma}_0$, (3) the steady rolling at $\dot{\gamma} = 0.6\dot{\gamma}_0$. (b) Velocity of the capsule's shell center of mass along the trajectories shown in (a). $\Phi = 0.62$, $E = 0.061$, $k_{off}/\dot{\gamma}_0 = 7.6$.

motion. It is worth noting that although the velocity of the capsule fluctuates in time (see Fig. 3b), the velocity of nodes is always close to zero near the substrate.

Our simulations successfully reproduce the three dynamic regimes observed in experimental studies on living cells, namely, the "stationary", "saltation" and "rolling" regimes.[41] It is important to note that our simulations are capable of reproducing the stationary and saltation regimes because the capsule-substrate interactions are described by the Bell model, which mimics the formation of the ligand-receptor bonds.[12,13] In contrast, if the energy-conserving Morse potential is used to model the capsule-substrate interactions, the capsule moves even under a weak shear flow; the capsule motion can, however, be arrested if the surfaces encompass chemical patterns or physical corrugations.[4,7] Below, we show that a capsule interacting with a substrate *via* Bell bonds can remain stationary even on a chemically homogeneous, smooth surface provided that the latter substrate is sufficiently soft.

3.2 Effect of substrate compliance on the rolling motion of the capsule

By varying the relative rigidity of the substrate, $E = E_{sub}/E_{cap}$, we found that the capsule is capable of rolling only on a sufficiently
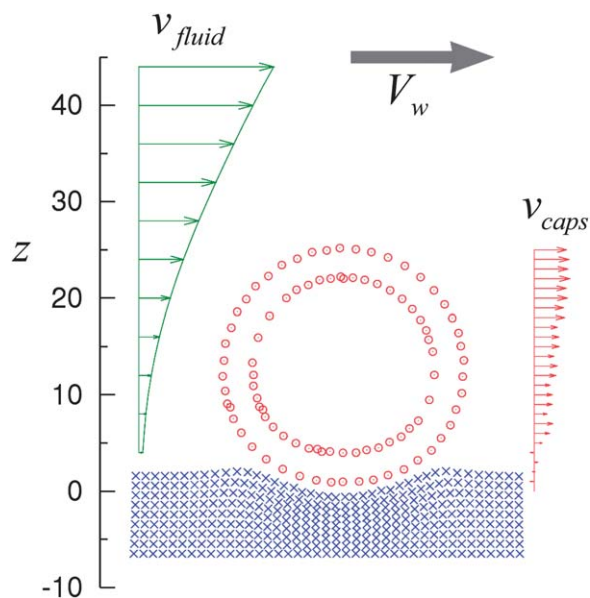

Fig. 4 The regime of steady rolling. The velocity profiles of fluid, v_{fluid}, and capsule, v_{caps}, and the configuration of the capsule (circles) and substrate (crosses) correspond to the middle of the simulation run (3) in Fig. 3 at $t = 1.1 \times 10^6 \, \Delta t_{LBM} = 2.4\dot{\gamma}_0^{-1}$.

rigid substrate. Fig. 5 shows the mean velocity v of the capsule's center of mass (averaged over 1.5 million time steps) as a function of E at the shear rate of $\dot{\gamma} = 0.15\dot{\gamma}_0$ and the two values of capsule rigidity of $\Phi_1 = 0.62$ (softer capsule) and $\Phi_2 = 0.5$ (stiffer capsule). Note that the substrate rigidity E_{sub} was normalized by the respective value of E_{cap}. Each data point shown in Fig. 5 represents an average over three or four independent simulation runs. The error bars indicate the standard deviation of the mean velocity. Fig. 5 shows that the dynamic behavior of fluid-driven capsules depends critically on the substrate rigidity. Namely, at a given shear rate $\dot{\gamma}$ and capsule rigidity Φ, the capsule moves if the value of E exceeds some critical value E_{cr}, and is stationary if
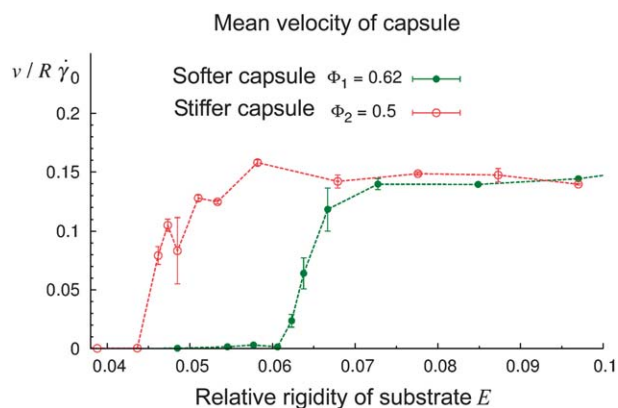

Fig. 5 Effect of the relative compliance of the substrate, $E = E_{sub}/E_{cap}$, on the velocity of rolling motion of the capsule at the capsule rigidity of $\Phi_1 = 0.62$ (softer capsule) and $\Phi_2 = 0.5$ (stiffer capsule). The results shown were obtained at $\dot{\gamma} = 0.15\dot{\gamma}_0$ and $k_{off}/\dot{\gamma}_0 = 7.6$. The data points were obtained by averaging the velocity over the last three-fourths of the simulation time.

$E < E_{cr}$. The value of E_{cr} decreases with an increase in the capsule rigidity, i.e., stiffer capsules can move on softer substrates. For a relative substrate rigidity E within the range of 0.058 to 0.061, the stiffer capsule $\Phi_2 = 0.5$ moves while the softer capsule $\Phi_1 = 0.62$ is in the stationary state (Fig. 5). At $0.061 \leq E \leq 0.064$, both of the capsules roll, but the stiffer capsule moves faster than the softer one. (It is worth noting that according to the Mann–Whitney–Wilcoxon test,[42] the difference in the mean velocity values is significant at the level of 5% within the latter range of E.) Finally, at a higher substrate rigidity of $E \geq 0.07$, both of the capsules move with the same velocity of $\approx 0.15\dot{\gamma}_0 R$, i.e., the velocity of the shear flow at the distance R from surface, $\dot{\gamma}R$.

If a capsule is in the stationary state on a soft substrate, a sufficient increase in the shear rate can drive the capsule to roll. Fig. 6 shows a phase map of the rolling and stationary regimes in the coordinates E and $\dot{\gamma}$ for a capsule of rigidity $\Phi = 0.62$. In Fig. 6, the circles and crosses denote the rolling and stationary regimes, respectively. As can be seen, the rolling regime is located at higher shear rates than the stationary regime, and the boundary between the two regimes is a decreasing function of substrate rigidity E. Hence, a higher shear rate $\dot{\gamma}$ is necessary to induce rolling on a soft substrate (low E) than on a stiff substrate.

The observed dependence of the dynamic behavior on the rigidity of both the capsule and substrate (Fig. 5 and 6) can be readily explained. Due to adhesion, both the capsule and substrate undergo a deformation (see Fig. 4). The more compliant the adherent surfaces are, the more adhesive bonds that are formed. As a result, a greater drag force is needed to break the bonds and drive the capsule to move. It is also clear that the motion of a capsule in shear flow should depend on how readily the capsule-surface bonds can be broken. The effect of the bond breakage rate is discussed in the next section.

3.3 Effect of the rate of bond breakage

Fig. 7a shows the trajectories of the capsule at values of the off-rate constant k_{off} varying from $1.5\dot{\gamma}_0$ to $7.6\dot{\gamma}_0$; the on-rate constant is fixed at $k_{on} = 10^{-3} \Delta t_{LBM}^{-1} = 450\dot{\gamma}_0$. To obtain the results presented in Fig. 7a, a capsule of rigidity $\Phi = 0.62$ was driven by an imposed shear rate of $\dot{\gamma} = 0.16\dot{\gamma}_0$ along a substrate of relative rigidity $E = 0.073$. The plot indicates that the
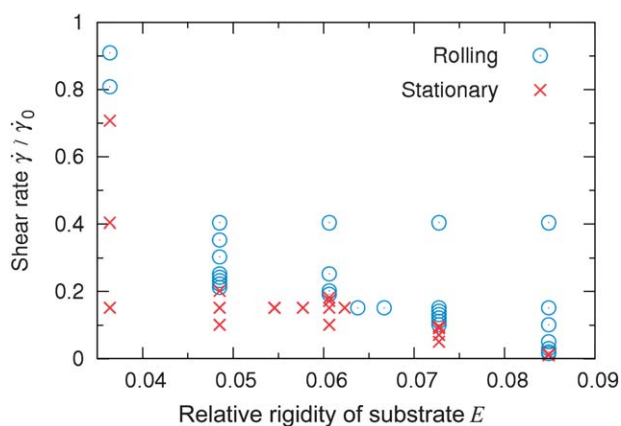
dynamics of bond breakage and formation can affect the regime of capsule motion on this substrate. In particular, Fig. 7a shows that the capsule motion is stationary at a low rate constant of the bond breakage (curve 1), and that an increase in k_{off} enables this capsule to roll on the surface (curves 2–5).[43]

It is important to note that the steady rolling motion was observed only in simulations involving sufficiently high breakage rates; in Fig. 7a, curves 4 and 5 correspond to the rolling regime. At intermediate values of k_{off}, the capsule exhibits irregular motion during which the capsule stops and then, starts moving again, as in curves 2 and 3 in Fig. 7a. This is the characteristic feature of the saltation regime. For a fixed set of parameters, the behavior of the capsule varies between different simulation runs in the saltation regime as demonstrated in Fig. 7b, which shows the trajectories obtained in three simulation runs at $k_{off} = 2.7\dot{\gamma}_0$. Furthermore, an increase in k_{off} does not necessarily result in a systematic increase in the velocity of the capsule in the saltation regime (not shown); this is in contrast to the behavior observed in the steady rolling regime.

The irregularity of capsule motion in the saltation regime is a manifestation of the fluctuations induced by the Bell bonds, which break and reform stochastically. At each time step in the
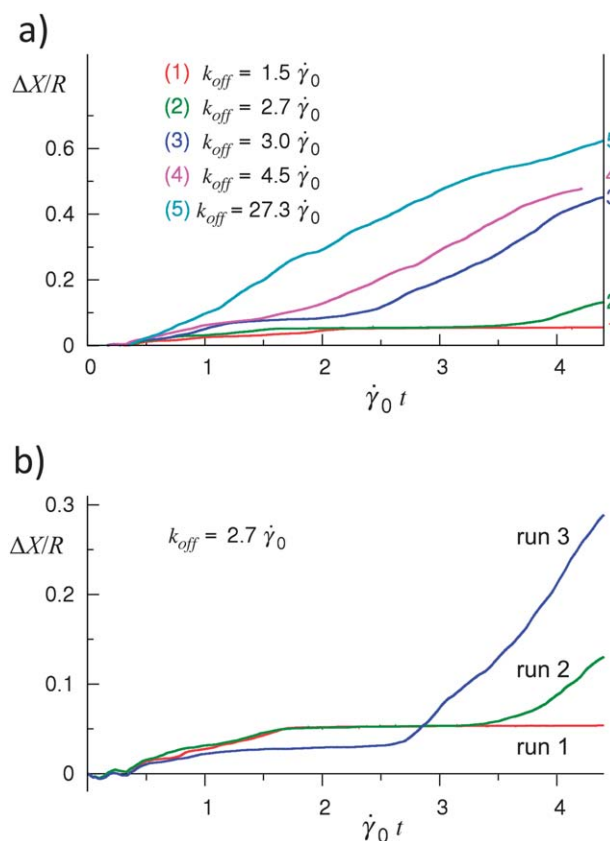

Fig. 7 Effect of the rate of bond breakage on the capsule's motion. (a) Displacement of the capsule's shell center of mass as a function of time at the values of k_{off} indicated in the figure. Depending upon k_{off}, the capsule exhibits the stationary state (curve 1), saltation (curves 2 and 3), or steady rolling (curves 4 and 5). (b) Irregularity of the capsule motion in the saltation regime: the behavior varies between different simulation runs. $\Phi = 0.62$, $E = 0.073$, $\dot{\gamma} = 0.16\dot{\gamma}_0$.

Fig. 6 Phase map of the rolling (circles) and stationary (crosses) regimes in the coordinates E and $\dot{\gamma}$ at $\Phi = 0.62$ and $k_{off}/\dot{\gamma}_0 = 7.6$.

simulations, there are from 5×10^3 to 1.5×10^4 bonds formed between the capsule and substrate; however, only a small fraction of these bonds affect the rolling of the capsule. The latter observation is evident from Fig. 8, which shows the probability of a bond to break as a function of the bond position at $k_{off} = 2.7\dot{\gamma}_0$. The bond breakage, which is necessary for the capsule to move, takes place predominantly at the rim of capsule-substrate contact area. Thus, only bonds located at the rim control the capsule rolling motion and cause the irregular dynamics in the saltation regime.

Fig. 9 summarizes the results of the simulations at various values of k_{off} and $\dot{\gamma}$, and the rigidities of the capsule and substrate of $\Phi = 0.62$ and $E = 0.073$, respectively. In this figure, the symbols indicate a regime of motion observed at a specific pair of values k_{off} and $\dot{\gamma}$. For each (k_{off}, $\dot{\gamma}$) pair, we ran three simulations and each simulation was run for 2×10^6 time steps, which corresponds to approximately 0.21 s of real time (see Section 2.2). The regime was labeled as "rolling" if the capsule moved steadily without stopping until the end of each of the three runs, and cases where the capsule was initially immobile up to 10^6 time steps were included. The regime was labeled as "stationary" if by the end of each of the three runs the capsule velocity was zero, and the cases of initial saltation were included. The regime was labeled as "saltation" in all other cases. The plot in Fig. 9 indicates that an increase in the off-rate k_{off} gives rise to a weaker capsule-substrate adhesion so that the capsule can move under lower shear rates.

4.   Conclusions

By integrating mesoscale computational approaches for modeling hydrodynamics, micromechanics, and adhesion, we investigated the fluid driven motion of an elastic microcapsule reversibly bound to a compliant surface. Our combined LBM/ LSM approach captures the dynamic interaction between the elastic capsule, substrate, and surrounding fluid, which is subject to the external shear. The adhesion between the capsule's shell and the substrate was due to the formation of biomimetic, reversible bonds, which were described by the Bell model.

Using this computational model, we observed three regimes of capsule motion. Namely, the capsule rolls steadily along the
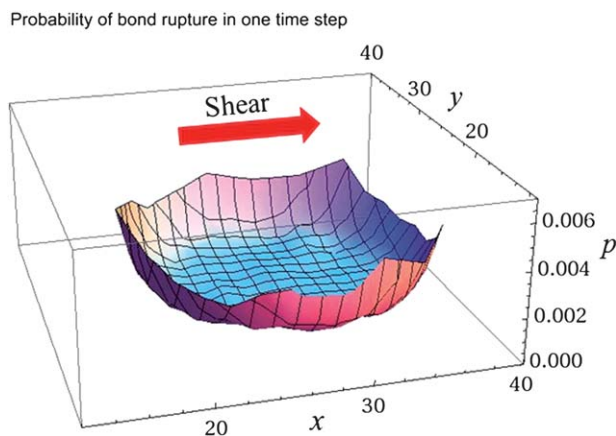

Fig. 8 The probability of a bond to break, w_r (see eqn (6)), as a function of bond position at $k_{off} = 2.7\dot{\gamma}_0$, $\Phi = 0.62$, $E = 0.073$, $\dot{\gamma} = 0.16\dot{\gamma}_0$.
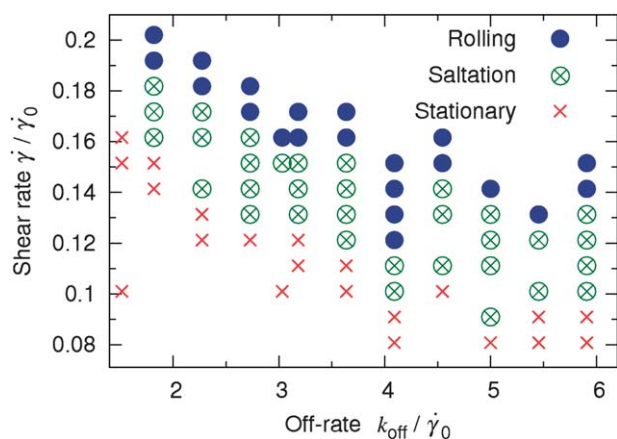

Fig. 9 Phase map of the stationary (crosses), saltation (crossed open circles), and rolling (solid disks) regimes of capsule motion in the coordinates k_{off} and $\dot{\gamma}$ at $\Phi = 0.62$ and $E = 0.073$.

substrate at a sufficiently high shear rate, it is stationary at a low shear rate, and exhibits an intermittent motion (saltation) at intermediate shear rates. At a given shear rate, the regime of capsule motion was found to depend on the substrate stiffness, and on the rate of rupture of the adhesive bonds. The capsule was observed to roll steadily on a sufficiently stiff substrate, and at a high rate of bond rupture. In the opposite limit of a soft substrate and a low rate of bond rupture, the system was localized in the stationary regime.

Within the range of model parameters considered here, the saltation regime is most clearly distinguished through a variation of the rate of bond rupture. We demonstrated that the irregular capsule motion characteristic of saltation is due to the stochasticity in the processes of bond rupture and formation. The irregular saltation motion exists even at a high surface density of the adhesive bonds. The latter behavior is due to the fact that not all of the bonds contribute to the capsule's dynamics; rather, it is only the fraction of bonds situated at the rim of the contact area that is primarily responsible for the motion of the capsule.

One of the motivations for carrying out these studies was to demonstrate that the compliance of the substrate can play a critical role in the dynamic behavior of the capsules. As noted above, we observed that a sufficiently rigid substrate is necessary for the sustained fluid-driven motion of the capsules. In other words, even in an imposed flow field, the capsules can be made to remain stationary by tailoring the compliance of the substrate. The latter findings are particularly important when considering the release of species encased within the capsules; namely, soft surfaces will favor the release of the encapsulated species in a specific area, while more rigid substrates will enable the released species to be effectively spread over a large region of the surface. In applications where the surface rigidity is not a variable, our findings show that the values of k_{off} and $\dot{\gamma}$ can be used to tailor the motion of the capsules. For example, for small k_{off} values (which can be achieved by judicious choice of functional groups on the capsules and surface), the capsules can remain stationary on a relatively rigid surface for a range of shear rates and again, the micro-carriers can thus be induced to deliver their contents to specific locations on the substrate. We note that the latter considerations are particularly important for drug delivery

applications. More generally, our findings can provide design rules for tailoring the efficacy of micro-carriers in transporting the encapsulated species to localized sites or broad regions on a substrate.

Acknowledgements

References

1 O. I. Vinogradova, *J. Phys.: Condens. Matter*, 2004, **16**, R1105–R1134.
2 N. Maurer, D. B. Fenske and P. R. Cullis, *Expert Opin. Biol. Ther.*, 2001, **1**, 1–25.
3 B. M. Discher, Y.-Y. Won, D. S. Ege, J. C.-M. Lee, F. S. Bates, D. E. Discher and D. A. Hammer, *Science*, 1999, **284**, 1143–1146.
4 A. Alexeev, R. Verberg and A. C. Balazs, *Macromolecules*, 2005, **38**, 10244–10260.
5 A. Alexeev, R. Verberg and A. C. Balazs, *Phys. Rev. Lett.*, 2006, **96**, 148103.
6 A. Alexeev and A. C. Balazs, *Soft Matter*, 2007, **3**, 1500–1505.
7 A. Alexeev, R. Verberg and A. C. Balazs, *Langmuir*, 2007, **23**, 983–987.
8 O. B. Usta, A. Alexeev and A. C. Balazs, *Langmuir*, 2007, **23**, 10887–10890.
9 G. V. Kolmakov, R. Revanur, R. Tangirala, T. Emrick, T. P. Russell, A. J. Crosby and A. C. Balazs, *ACS Nano*, 2010, **4**, 1115–1123.
10 S. Succi, *The lattice Boltzmann equation for fluid dynamics and beyond*, Oxford University Press, Oxford, 2001.
11 G. A. Buxton, C. M. Care and D. J. Cleaver, *Modell. Simul. Mater. Sci. Eng.*, 2001, **9**, 485–497.
12 G. I. Bell, *Science*, 1978, **200**, 618–627.
13 M. Dembo, D. C. Torney, K. Saxman and D. Hammer, *Proc. R. Soc. London, Ser. B*, 1988, **234**, 55–83.
14 S. K. Bhatia, M. R. King and D. A. Hammer, *Biophys. J.*, 2003, **84**, 2671–2690.
15 V. Pappu and P. Bagchi, *Comput. Biol. Med.*, 2008, **38**, 738–753.
16 G. A. Buxton, R. Verberg, D. Jasnow and A. C. Balazs, *Phys. Rev. E*, 2005, **71**, 056707–18.
17 S. Duki, G. V. Kolmakov, V. V. Yashin, T. Kowalewski, K. Matyjaszewski and A. C. Balazs, *J. Chem. Phys.*, 2011, **134**(8), 084901.
18 Y. H. Qian, D. D'Humières and P. Lallemand, *Europhys. Lett.*, 1992, **17**, 479–484.
19 (*a*) R. Cornubert, D. D'Humieres and D. Levermore, *Phys. D*, 1991, **47**, 241–259; (*b*) P. Lallemand and L.-S. Luo, *Phys. Rev. E*, 2000, **61**, 6546–6562.
20 For the model parameters used in the simulations, we never approach the regime where overlapping is possible and thus, it is not necessary to use a potential that exhibits a divergence (as the separation distance approaches zero). Namely, the shear rates are sufficiently small that the distance between the capsule and the substrate nodes varies around its equilibrium value. Therefore, a description of the potential at distances much shorter than the latter equilibrium distance is not essential in our simulations.
21 M. D. Ward, M. Dembo and D. A. Hammer, *Biophys. J.*, 1994, **67**, 2522–2534.
22 E. Evans and K. Ritchie, *Biophys. J.*, 1997, **72**, 1541–1555.
23 T. Strunz, K. Oroszlan, I. Schumakovitch, H.-J. Güntherodt and M. Hegner, *Biophys. J.*, 2000, **79**, 1206–1212.
24 M. J. Buehler, S. Keten and T. Ackbarow, *Prog. Mater. Sci.*, 2008, **53**, 1101–1241.
25 M. Rief, M. Gautel, F. Oesterhelt, J. M. Fernandez and H. E. Gaub, *Science*, 1997, **276**, 1109–1112.
26 T. J. Wickham, R. R. Granados, H. A. Wood, D. A. Hammer and M. L. Shuler, *Biophys. J.*, 1990, **58**, 1501–1516.
27 B. Zhang, T. S. Lim, S. R. K. Vedula, A. Li, C. T. Lim and V. B. C. Tan, *Biochemistry*, 2010, **49**, 1776–1786.
28 R. Alon, D. A. Hammer and T. A. Springer, *Nature*, 1995, **374**, 539–542.
29 M. R. King and D. A. Hammer, *Proc. Natl. Acad. Sci. U. S. A.*, 2001, **98**, 14919–15924.
30 L. S.-L. Cheung, X. Zheng, L. Wang, J. C. Baygents, R. Guzman, J. A. Schroeder, R. L. Heimark and Y. Zohar, *J. Micromech. Microeng.*, 2011, **21**, 054033.
31 A. Fery, F. Dubreuil and H. Möhwald, *New J. Phys.*, 2004, **6**, 18.
32 V. T. Moy, E.-L. Florin and H. E. Gaub, *Science*, 1994, **266**, 257–259.
33 A. P. Wiita, S. R. K. Ainavarapu, H. H. Huang and J. M. Fernandez, *Proc. Natl. Acad. Sci. U. S. A.*, 2006, **103**, 7222–7227.
34 M. A. Hjortso and J. W. Roos (ed.), *Cell adhesion: Fundamentals and Biotechnological Applications*, Marcel Dekker, 1995.
35 C. Andersen, M. Jordy and R. Benz, *J. Gen. Physiol.*, 1995, **105**, 385–401.
36 M. A. Hachem, E. N. Karlsson, E. Bartonek-Roxå, S. Raghothama, P. J. Simpson, H. J. Gilbert, M. P. Williamson and O. Holst, *Biochem. J.*, 2000, **345**, 53–60.
37 C. Obrecht, F. Kuznik, B. Tourancheau and J.-J. Roux, *Comput. Math. Appl.*, 2011, **61**(12), 3628–3638.
38 A. J. C. Ladd, *J. Fluid Mech.*, 1994, **271**, 285–309.
39 J. Latt and B. Chopard, *Math. Comput. Simul.*, 2006, **72**, 165–168.
40 G. B. Zibari, M. F. Brown, D. L. Burney, N. Granger and J. C. McDonald, *Transplant. Proc.*, 1998, **30**, 2327–2330.
41 K.-C. Chang, D. F. J. Tees and D. A. Hammer, *PNAS*, 2000, **97**, 11262–11267.
42 S. M. Ross, *Introductory statistics*, vol. 1, Elsevier Academic Press, 2005.
43 The number of breaking events during the time it takes the capsule to displace its own radius is a meaningful characteristic of the system; however, this parameter is well defined only in the steady rolling regime, which takes place at sufficiently high values of k_{off}. Hence, to present the data in Fig. 7 and 9, we normalize k_{off} using the reference shear rate $\dot{\gamma}_0$; the latter combination is well defined in all of the observed regimes.